

# Meso-structure in three strong-lensing systems

Prasenjit Saha

*Institute for Theoretical Physics, University of Zürich,  
Winterthurerstrasse 190, 8057 Zürich, Switzerland*

Liliya L.R. Williams

*Department of Astronomy, University of Minnesota,  
116 Church Street SE, Minneapolis, MN 55455*

Ignacio Ferreras

*Physics Department, King's College London  
Strand, London WC2R 2LS, UK*

## ABSTRACT

We map substructure in three strong lensing systems having particularly good image data: the galaxy lens MG J0414+053 and the clusters SDSS J1004+411 and ACO 1689. Our method is to first reconstruct the lens as a pixelated mass map and then subtract off the symmetric part (in the galaxy case) or a projected NFW (for the cluster lenses). In all three systems we find extended irregular structures, or meso-structures, having of order 10% of the total mass. In J0414+053, the meso-structure suggests a tidal tail connecting the main lens with a nearby galaxy; however this interpretation is tentative. In the clusters the identification of meso-structure is more secure, especially in ACO 1689 where two independent sets of lensed images imply very similar meso-structure. In all three cases the meso-structures are correlated with galaxies but much more extended and massive than the stellar components of single galaxies. Such extended structures cannot plausibly persist in such high-density regions without being mixed; the crossing times are too short. The meso-structures therefore appear to be merging or otherwise dynamically evolving systems.

*Subject headings:* gravitational lensing — galaxies: clusters: individual (SDSS J1004+411, ACO 1689)

## 1. Introduction

It is a commonplace nowadays that astrophysical systems once thought to be isolated and quiescent turn out to have complicated substructures that are evolving now. To give just two recent examples: Belokurov et al. (2006) discern two wraps of the Sagittarius Dwarf galaxy as it merges into the halo of the Milky Way, while in the Coma cluster Adami et al. (2005) identify 17 different galaxy groups.

Substructure has long been of special interest in gravitational lensing systems, because of the prospects of detecting dark matter substructure. An early example is Bartelmann et al. (1995) who argue that mass substructure in clusters is necessary to explain the observed distribution and properties of arcs. Later Mao & Schneider (1998) noted that mass substructure (on much smaller mass and length scales than in the case of clusters) readily explains the observed magnification ratios in a galaxy lens, and more recently this topic has attracted more attention. There is general agreement that substructure and microlensing are both present and both contribute to anomalous flux ratios in galaxy lenses, but there is considerable debate as to whether the expected CDM substructure can account for the observations (Dalal & Kochanek 2002; Metcalf & Zhao 2002; Evans & Witt 2003; Bradač et al. 2004; Amara et al. 2006; Macciò & Miranda 2006). Such comparison of observed and model-predicted flux ratios is entirely statistical; it does not attempt to map particular substructures, as the mass of individual clumps is rather small, in the range  $10^4 - 10^7 M_\odot$ . On the other extreme, some galaxies and clusters have substructures comparable to the size of the whole lens. For example, if a lens consists of two or more distinct components of comparable mass, uncovering these is relatively straightforward (Abdelsalam et al. 1998a,b; Gray et al. 2002). The most elusive type of substructure is that which comprises roughly 10% of the lens mass, but has a considerable covering factor, or order of 50%. Until recently only tentative maps of such structures have been possible (Williams & Saha 2004).

In this paper we map and interpret substructure in three lensing systems with exceptionally good lensing data. Previous work has identified substructure in all three systems, but here we will go into more details. The first system is the galaxy lens J0414+053, which is a quad unique for the magnification information it provides. Trotter et al. (2000) resolved the lensed images using VLBI to  $\sim 0.01''$ , revealing multiple components, and hence supplying tensor relative magnifications between the images. The second system is cluster SDSS J1004+411, which has 14 images from four sources (Sharon et al. 2005) and even a time delay measurement (Fohlmeister et al. 2006). The third system is the inner region of ACO 1689, well known as an exceptionally rich lensing cluster, where Broadhurst et al. (2005) have now identified 30 separate lensed sources giving rise to over 100 images in all.

## 2. The galaxy lens MG J0414+053

J0414+053 is a quad where each image has multiple components  $\sim 0.01''$  apart. The main lens is an early type galaxy G, but there is also a second, fainter galaxy X that also contributes to the lens. There are two independent sets of VLBI observations, with associated models. Ros et al. (2000) identify at least two distinct components in the quadruply-imaged source, and fit the image positions and flux ratios with two isothermal spheres plus external shear. Trotter et al. (2000) go even further, identifying four source components and developing a lens model made up of basis functions that fits the source substructure in detail.

Resolved image components provide information on magnification beyond flux ratios. Recall that the magnification tensor  $\vec{M}$  relates a source differential  $d\vec{\beta}$  and the corresponding image differential  $d\vec{\theta}$  by

$$d\vec{\theta} = \vec{M} d\vec{\beta}. \quad (1)$$

At another image from the same source there will be a different magnification tensor  $\vec{M}'$ , leading to a different image differential

$$d\vec{\theta}' = \vec{M}' d\vec{\beta}. \quad (2)$$

Since the source differential is common we have

$$d\vec{\theta}' = \vec{M}' \vec{M}^{-1} d\vec{\theta}. \quad (3)$$

For unresolved sources the flux ratio is  $\det |\vec{M}' \vec{M}^{-1}|$ . On the other hand, resolved sources can measure the tensor relative magnification  $\vec{M}' \vec{M}^{-1}$ . This point was made by Gorenstein et al. (1984) and their Eq. (2) is essentially our Eq. (3). They and later authors used the idea to incorporate tensor magnification in models of B0957+561 (Garrett et al. 1994; Grogin & Narayan 1996) and B1422+231 (Raychaudhury et al. 2003).

To the Gorenstein et al. (1984) result we may add that explicit calculation of the tensor magnification is not necessary. If three non-colinear features in the source are resolved in the images, they provide two linearly independent source displacements, and hence the relative tensor magnification is automatically constrained. In practice there are caveats: the source components may be nearly colinear, especially if they are knots in an AGN jet; or the magnification itself may vary across the source. So it is desirable to have more resolved features. Nevertheless, if a model reproduces the image positions for a three-component source, it can reasonably claim to have fitted the tensor magnification. With four images having four components each, J0414+053 arguably provides the most detailed magnification information of any galaxy lens. Trotter et al. (2000) implicitly fitted the tensor magnifications in their models. However, they did not inspect their free-form model in greater detail to see

if the second galaxy X or other substructures were buried in it. It would be interesting to reconstruct and post-process their published models in this way. However, in this paper we start from their VLBI image maps and remodel the lens using a different free-form modeling method.

We use the *PixeLens* modeling code (Saha & Williams 2004) which generates ensembles of pixelated 2D mass maps that (a) exactly reproduce the given image positions and, where known, time delays between images, and (b) are consistent with a prior. The data in question are the image positions. The prior requires (i) the mass pixels to be non-negative; (ii) density gradient anywhere to point within  $45^\circ$  of the lens center; (iii) any mass pixel to have at most twice the average density of its neighbors, except for the central pixel which is unlimited; (iv) the circularly averaged mass profile to be steeper than  $R^{-0.5}$ . The lens center is assumed to coincide with the galaxy light peak, but no other information about the galaxy light is supplied. This prior is designed to incorporate some conservative assumptions about the lenses. The earlier paper includes more justification of the prior, while Saha et al. (2006a) tests the prior against a galaxy-formation simulation.

Fig. 1 shows our mass map for J0414+053, actually the average of an ensemble of 400 mass models.<sup>1</sup> The input data were the positions of the image components p,r,s from Fig. 2 and Table 1 of Trotter et al. (2000), along with lens and source redshifts and the centroid of the main lensing galaxy G. (A fourth component, q, is very close to p, and not considered separately in our models.) The mass map shows an asymmetry with more mass in the proximity of the second galaxy X. Since X is only  $\sim 10\%$  as bright as G and the models had no input on X, it would be very interesting if the models infer substructure associated with X. But before going on to substructure, let us examine the models some more.

In Fig. 2 we show the model tensor magnifications with ellipses. Analogous ellipses appear in Fig. 3 of Trotter et al. (2000), and from visual comparison the results seem consistent. The ellipses are oriented nearly radial-tangential with respect to the center of G, but not quite: for image 2 the misalignment is  $\sim 1^\circ$ , while for the other images it is  $5\text{--}7^\circ$ . The orientations vary only  $\sim 1^\circ$  across the model ensemble, despite considerable variation in the mass maps themselves. Evidently the orientation of the magnification is strongly constrained by the VLBI positions.

Now consider specifically inverse radial magnification  $1 - \psi_{rr}$ , where  $\psi$  is the lens potential. In the ensemble-average model this quantity is in the ratio 0.95:1:0.88:0.78 for images 1 through 4. The ratios vary across the ensemble, but images 2–4 consistently have their inverse radial magnifications in decreasing order. This is of interest because the generalized

---

<sup>1</sup>See the Appendix for further details on the interpretation of model ensembles and ensemble-averages.

isothermal potentials (Witt et al. 2000) widely used in parametric models of galaxy lenses predict that the radial magnification should be equal for all images. Could the total lens potential here consist of a generalized isothermal for the main lens, plus a small perturbation from galaxy X? If so we would expect images 2–4, which are far from X, to all have equal radial magnification, which is not the case. So, it appears that even without X the lens is not a generalized isothermal. If galaxy-lens potentials are in general significantly different from generalized isothermals, then conclusions derived using this assumption (Congdon & Keeton 2005; Yoo et al. 2005, 2006) may need to be revised. A useful test would be to see whether a generalized isothermal plus a perturbation from X can fit the VLBI image structure in J0414+053.

Fig. 3 plots the enclosed mass against projected radius. We see that the total mass within the region of the images is well-constrained, but the data allow the mass profile to be shallow or steep. This is simply an illustration of the well-known steepness degeneracy that afflicts all lens models from a single source redshift. (See e.g., Saha & Williams 2006, for a recent discussion of degeneracies.)

Because of the uncertainty in the mass profile, it is difficult to define a base profile that can be subtracted off to isolate the substructure. We therefore define a simple residual,

$$\Sigma(\vec{\theta}) - \min [\Sigma(\vec{\theta}), \Sigma(-\vec{\theta})] . \quad (4)$$

Here the second term is the maximal inversion-symmetric profile that is non-negative everywhere. The whole expression may be called the asymmetric overdensity. It is shown in Fig. 4. The apparent coincidence of one overdensity with the secondary galaxy X is intriguing. Are we seeing part of a tidal tail?

We estimated the stellar mass in galaxies G and X using the observed magnitudes and colors from CASTLeS<sup>2</sup> and standard population-evolution models, using the method described in Ferreras et al. (2005), which yields  $\sim 5 \times 10^{11} M_{\odot}$  for G and  $\sim 5 \times 10^{10} M_{\odot}$  for X. The former is roughly half the total lensing mass, while the latter is roughly half the mass of the substructure. The interpretation of X as a satellite galaxy merging into the halo of G seems plausible. But it must be considered tentative.

---

<sup>2</sup><http://www.cfa.harvard.edu/glensdata/>

### 3. The cluster SDSS J1004+411

This cluster initially attracted attention as a host of a giant quadruple quasar (Inada et al. 2003; Oguri et al. 2004). Subsequent data have been greatly enhanced by the discovery of a central image of the quasar (Inada et al. 2005), a time-delay measurement (Fohlmeister et al. 2006) and most importantly the discovery of three new multiply-imaged galaxies (Sharon et al. 2005). The latter work provides 9 new images with a range of redshifts and covering a larger area than the original quasar images; it also develops a mass model with a slowly varying smooth part and discrete components associated with galaxies, which fits all the image data.

An early attempt to map the substructure in this cluster was made in Williams & Saha (2004) using just the four quasar-image positions then available. The results varied with the priors used (four priors were illustrated) and the conclusions relied on indirect arguments. The paper argued for a shallow mass profile with up to 10% of the mass in substructure, with the substructure spatially correlated with galaxies. In hindsight these conclusions appear broadly correct. The paper also favored models where the short time-delay was  $\leq 20$  d and the external mass had a roughly E/W long axis over models with longer time delays and/or a roughly N/S axis for the external mass, but these conclusions were incorrect—the short time delay for the quasar is measured as  $38.3 \pm 2$  d, while the quintuply-imaged galaxy shares the typical morphology of short-axis quads (Saha & Williams 2003) indicating the external mass axis to be roughly NWN or SES.

The problems encountered in Williams & Saha (2004) largely disappear once we include the new multiple-imaged systems from Sharon et al. (2005). (Saha et al. 2006b, ; hereafter Paper I) presents an ensemble of models fitting 13 images from the four known sources. (One of the two central images is omitted because of resolution limits in the code.) The technique is the same as we used above for J0414+053, except for two important differences:

1. The minimal steepness requirement of  $R^{-0.5}$  is dropped, since for clusters a shallower profile is expected than for galaxies.
2. The range in  $z_s$  is incorporated. The availability of a range of  $z_s$  breaks the steepness degeneracy (Abdelsalam et al. 1998b) seen in Fig. 3 above and which plagues galaxy-lensing generally.

The prior is weaker than any of the priors in Williams & Saha (2004), yet the mass profile and the mass map in general are much better constrained. Paper I concentrates on the circularly-averaged mass profile, finding it to agree with the inner profiles typical of cold dark matter simulations, postponing the study of substructure. But we remark that in the models of J1004+411 in Paper I, the short time delay ranges from 0 to 60 d (in other words,

it is not well-constrained but is consistent with the measured value), while the fitted external shear implies the long axis of external mass to be NWN/SES.

Adding the time-delay as a constraint is straightforward. In Fig. 5 we show the ensemble-average of 400 models fitting the measured time delay as well as the 13 images from four sources. Comparing with Fig. 1 in Paper I shows only very small differences. In other words, once the three additional image-systems have been incorporated, the short time-delay makes only a small incremental difference. The Fohlmeister et al. (2006) measurement is nevertheless important, because it sets a baseline for future measurements of the longer delays, which will provide stronger constraints on the mass distribution and possibly an accurate single-lens measurement of  $H_0$ .

Proceeding now to substructure, we subtract off the best-fit NFW profile from the mass map. That is to say, we fit the projected form (Bartelmann 1996) of the spherical NFW profile to Fig. 5 and subtract it off. One can imagine other, perhaps better, procedures for uncovering substructure, but this one seems the simplest. We do the same with the mass map of J1004+411 from Paper I, which lacks the time-delay constraint and uses slightly larger pixels. Fig. 6 shows the results.<sup>3</sup> We see overdensity mostly to the N and S. This is broadly consistent with the substructure maps over a smaller area in Williams & Saha (2004), which used a different method to subtract off the smooth portion. Fig. 6 overplots the probable cluster galaxies. These are galaxies brighter than  $i = 24$ , with a color cut following Oguri et al. (2004). From Fig. 10 of that paper, we estimate the typical galaxy to have  $M_r \simeq -20.5$  or  $\sim 10^{10} L_\odot$ . We have not attempted a population-evolution model for the stellar mass, but the latter is probably less than the mass in the substructure ( $6\text{--}7 \times 10^{12} M_\odot$ ) and can be only a few percent of the total in the field.

Fig. 6 unfortunately also shows an artifact common in *PixeLens* mass maps. Although the density-gradient constraint in the prior (see Section 2) disallows mass peaks, the discretized form that is actually implemented disallows extended hills but allows one-pixel peaks. Usually this artifact is only noticeable as single-pixel blemishes (Saha & Williams 1997) but subtracting off a profile one-pixel peaks become proportionately higher. In particular, Fig. 6 shows a corrugation effect in some places, consisting of an array of one-pixel peaks.

Are the galaxies correlated with the substructure? It is easy to make a statistical test for this (an improved version of the test used in Williams & Saha 2004) as follows. Take the total lens mass within a projected distance  $R$  of each galaxy, and sum over all galaxies (weighted

---

<sup>3</sup>Recall that Fig. 6 refers to the average of an ensemble of 400 models. See Fig. 12 for results from smaller ensembles, down to a single model.

by the galaxy brightness if available). Call this  $h(R)$ . Next, calculate  $\tilde{h}(R)$  by rotating each galaxy around the cluster center by a random angle. Let  $S(R)$  be the percentage of cases where  $\tilde{h}(R) < h(R)$ . We may call this the percentage significance.<sup>4</sup> If  $S(R)$  is close to 100% then the galaxies are correlated with non-radial variations in the density, that is, with substructure.

Fig. 7 shows that galaxies are correlated with substructure to scales of  $\sim 50$  kpc. (Short range correlation is not significant because the mass reconstruction is noisy on the pixel-to-pixel scale.) Note that the correlation does not mean that most of the galaxies are associated with overdensities, it only implies that overdensity increases the chance there being a galaxy, even  $\sim 100$  kpc away. The overdensities must hence be interpreted as genuine extended structures, not statistical associations of much smaller structures. Hence the term *meso-structure*.

Now the total cluster density at  $r \sim 100$  kpc is  $\simeq 4 \times 10^6 M_\odot \text{ kpc}^{-3}$  (cf. Paper I). This gives a crossing time  $(G\rho)^{-\frac{1}{2}} \simeq 2 \times 10^8 \text{ yr}$ , much shorter than the age of the cluster. Hence meso-structure of  $\sim 10\%$  of the total mass on a scale of  $\sim 100$  kpc would have gotten mixed long ago. Thus the observed meso-structure seems most plausible as either a line-of-sight filament or as a merger in progress.

#### 4. The cluster ACO 1689

We saw above that the observations of J1004+411 allowed a more detailed and confident mapping of substructure. For ACO 1689 the situation is much better still: the observations (Broadhurst et al. 2005) are enough to reconstruct the lens twice from two different data sets; additionally, redshifts of individual cluster galaxies are available. As well as Broadhurst et al. (2005), several other groups have modeled these data (Diego et al. 2005; Zekser et al. 2006; Halkola et al. 2006; Limousin et al. 2006). These papers all agree that the cluster is compatible with an NFW profile plus some substructure, but the substructure itself has not been discussed in detail, apart from a distinctive clump to the NE. (This clump is oriented towards 2 o’clock in some published figures.)

Mass maps of the cluster using two sets of multiple images and using the same prior as for J1004+411 are presented in Paper I. Fig. 8 shows the result of subtracting off the

---

<sup>4</sup>Percentage significance is not a statistics term. What we call “95% significant” is known in statistics as “ $p$  value of 0.05”, and will be significant (or not) if it is less (or more) than the pre-specified significance *level*. But apart from the use of astronomers’ vernacular, our procedure is standard statistics.



best-fit NFW profile from these mass maps. Although our initial reason for modeling two subsets of the data that *PixeLens* currently cannot handle all the data together, we have here an unexpected bonus: similar substructure comes out of independent data sets. The NE clump and two other overdense regions are evident. Diego et al. (2005) mention three substructure clumps in passing, but we do not know if they identified the same ones.

Colors and redshifts of galaxies in the field have been tabulated by Duc et al. (2002). A break around  $B - R = 2$  is noticeable in the observed colors, and accordingly we suggest that galaxies redder than this are probable cluster members. Fig. 9 shows these galaxies. We have not attempted a population-evolution model, but a very rough extrapolation from Ferreras et al. (2005) indicates a few times  $10^{12} M_{\odot}$  in stellar mass, much less than the meso-structure. The meso-structure does, however, correlate with the galaxies, as Fig. 10 shows. As in J1004+411, we see correlations, but in this cluster they extend further, to  $\sim 100$  kpc scales or even beyond.

As with J1004+411, the most plausible interpretation of the  $\sim 10\%$  meso-structure is again as either line-of-sight filaments or as ongoing mergers.

We make an attempt to test for these possibilities. In Fig. 11 we show a perspective version of Fig. 9 with the third dimension being the redshift relative to the brightest cluster galaxy. There are no distinctive groups in this plot, so it does not appear that ACO 1689 consists of two or more isolated clusters. This appears to favor the filament interpretation.

## 5. Discussion

Our results leave no doubt that substructure at the 10% level can be mapped in the best-observed strong-lensing systems. The inferred substructure is tentative for the galaxy lens J0414+053, more confident for the cluster lens J1004+411, while for ACO 1689 the substructure is explicitly verified by using independent subsets of the data. It turns out that, although the link between magnification and substructure has attracted much attention recently, in fact multiple sources provide more information on substructure than magnification.

The substructure we find is meso-structure: extended features much larger than galaxies and more massive than the stellar content, but correlated with galaxies. Such features would not survive unmixed in the inner regions of the galaxies or clusters, and they are improbable as chance alignments. Evidently they are interacting or otherwise dynamically evolving.

Much more can be done with current or near-future data, especially in the case of ACO 1689. One important goal is to make the lens reconstructions finer grained. Here

progress using adaptive resolution has been made (Saha et al. 2001; Diego et al. 2005) but the real challenge is to resolve the halos of individual galaxies. A study of cluster-galaxy redshifts and the implied dynamics would help resolve the 3D structure. More understanding of the gas dynamics is needed, not least the puzzle of why the equilibrium models for x-ray gas underestimate the total mass (Andersson & Madejski 2004). These are all messy problems, but worth research effort, because the variety of data on ACO 1689 makes it perhaps our most hopeful place for understanding the physics of cluster and galaxy formation.

We thank Paul Schechter for the appropriate mix of encouragement and criticism, and for suggesting the term ‘meso-structure’.

### A. Inside the model ensembles

The results in this paper derive from ensembles of pixelated models. (We have five such ensembles: one for J0414+053, two from slightly different data on J1004+411, and two using disjoint data sets on ACO 1689. Each ensemble has 400 models.) Each model in an ensemble is required to reproduce the data precisely; subject to this constraint, the ensemble samples models according to the prior.

Such model ensembles are by now a standard technique in data analysis, described in several books (for example, Saha 2003), and known by different names such as Metropolis algorithm or Markov-Chain Monte-Carlo. The ensemble has the interpretation of a Bayesian posterior probability distribution for the model — which in our case is the mass map — and from this two very useful properties follow.

1. A histogram of any quantity (for example, the enclosed mass within 100 kpc) across the ensemble is the posterior probability distribution for that quantity, with all other variables marginalized out. Hence error bars, including asymmetric error bars, can be trivially extracted from the ensemble.
2. The ensemble average of any quantity is its expectation value. Thus the ensemble-average models we have illustrated have each pixel set to its expectation value.

The above properties apply also to other lens-ensemble methods (Keeton & Winn 2003; Oguri et al. 2004). However, *PixeLens* ensembles have a further useful property. Since the data constraints are expressed as linear equations and the prior is formulated as linear inequalities, it follows that the ensemble-average model automatically fits both data and

prior. The ensemble-average model in *PixeLens* is thus a very useful one to illustrate: it fits the data, satisfies the prior, and is also the expectation value across the whole ensemble.

The meso-structure results in the main part of this paper refer to the average models from ensembles of 400. It is interesting to also examine smaller averages over the ensemble, down to individual models. In Figure 12 we show the inferred meso-structure in J1004+411 if we take a single model, or average 4, 16, or 80 models, and then remove the best-fit projected NFW profile in each case. The no-average case shows a lot of pixel-to-pixel variation, which gradually fades as we take larger and larger averages. The unaveraged model still fits the data precisely, so the pixel-to-pixel variation is not noise in the usual sense. The variation appears and fades because in any one model some pixels will be at the tails of their respective probability distributions, whereas in an average all pixels are at their expectation values. Nevertheless, the meso-structure is discernable even in a single model, and becomes quite clear even in an average over 4 models.

We conclude that the meso-structure cannot be an artifact of ensemble-averaging.

## REFERENCES

- Abdelsalam, H. M., Saha, P., & Williams, L. L. R. 1998a, MNRAS, 294, 734
- . 1998b, AJ, 116, 1541
- Adami, C., Biviano, A., Durret, F., & Mazure, A. 2005, A&A, 443, 17
- Amara, A., Metcalf, R. B., Cox, T. J., & Ostriker, J. P. 2006, MNRAS, 367, 1367
- Andersson, K. E. & Madejski, G. M. 2004, ApJ, 607, 190
- Bartelmann, M. 1996, A&A, 313, 697
- Bartelmann, M., Steinmetz, M., & Weiss, A. 1995, A&A, 297, 1
- Belokurov, V., Zucker, D. B., Evans, N. W., Gilmore, G., Vidrih, S., Bramich, D. M., Newberg, H. J., Wyse, R. F. G., Irwin, M. J., Fellhauer, M., Hewett, P. C., Walton, N. A., Wilkinson, M. I., Cole, N., Yanny, B., Rockosi, C. M., Beers, T. C., Bell, E. F., Brinkmann, J., Ivezić, Ž., & Lupton, R. 2006, ApJ, 642, L137
- Bradač, M., Schneider, P., Lombardi, M., Steinmetz, M., Koopmans, L. V. E., & Navarro, J. F. 2004, A&A, 423, 797
- Broadhurst, T., Benítez, N., Coe, D., Sharon, K., Zekser, K., White, R., Ford, H., Bouwens, R., Blakeslee, J., Clampin, M., Cross, N., Franx, M., Frye, B., Hartig, G., Illingworth, G., Infante, L., Menanteau, F., Meurer, G., Postman, M., Ardila, D. R., Bartko, F., Brown, R. A., Burrows, C. J., Cheng, E. S., Feldman, P. D., Golimowski, D. A., Goto, T., Gronwall, C., Herranz, D., Holden, B., Homeier, N., Krist, J. E., Lesser, M. P., Martel, A. R., Miley, G. K., Rosati, P., Sirianni, M., Sparks, W. B., Steindling, S., Tran, H. D., Tsvetanov, Z. I., & Zheng, W. 2005, ApJ, 621, 53
- Congdon, A. B. & Keeton, C. R. 2005, MNRAS, 364, 1459
- Dalal, N. & Kochanek, C. S. 2002, ApJ, 572, 25
- Diego, J. M., Sandvik, H. B., Protopapas, P., Tegmark, M., Benítez, N., & Broadhurst, T. 2005, MNRAS, 362, 1247
- Duc, P.-A., Poggianti, B. M., Fadda, D., Elbaz, D., Flores, H., Chanical, P., Franceschini, A., Moorwood, A., & Cesarsky, C. 2002, A&A, 382, 60
- Evans, N. W. & Witt, H. J. 2003, MNRAS, 345, 1351

- Ferreras, I., Saha, P., & Williams, L. L. R. 2005, *ApJ*, 623, L5
- Fohlmeister, J., Kochanek, C. S., & Falco, E. 2006, [astro-ph/0607513](#)
- Garrett, M. A., Calder, R. J., Porcas, R. W., King, L. J., Walsh, D., & Wilkinson, P. N. 1994, *MNRAS*, 270, 457
- Gorenstein, M. V., Shapiro, I. I., Rogers, A. E. E., Cohen, N. L., Corey, B. E., Porcas, R. W., Falco, E. E., Bonometti, R. J., Preston, R. A., Rius, A., & Whitney, A. R. 1984, *ApJ*, 287, 538
- Gray, M. E., Taylor, A. N., Meisenheimer, K., Dye, S., Wolf, C., & Thommes, E. 2002, *ApJ*, 568, 141
- Grogin, N. A. & Narayan, R. 1996, *ApJ*, 464, 92
- Halkola, A., Seitz, S., & Pannella, M. 2006, *MNRAS*, 372, 1425
- Inada, N., Oguri, M., Keeton, C. R., Eisenstein, D. J., Castander, F. J., Chiu, K., Hall, P. B., Hennawi, J. F., Johnston, D. E., Pindor, B., Richards, G. T., Rix, H.-W. R., Schneider, D. P., & Zheng, W. 2005, *PASJ*, 57, L7
- Inada, N., Oguri, M., Pindor, B., Hennawi, J. F., Chiu, K., Zheng, W., Ichikawa, S.-I., Gregg, M. D., Becker, R. H., Suto, Y., Strauss, M. A., Turner, E. L., Keeton, C. R., Annis, J., Castander, F. J., Eisenstein, D. J., Frieman, J. A., Fukugita, M., Gunn, J. E., Johnston, D. E., Kent, S. M., Nichol, R. C., Richards, G. T., Rix, H.-W., Sheldon, E. S., Bahcall, N. A., Brinkmann, J., Ivezić, Ž., Lamb, D. Q., McKay, T. A., Schneider, D. P., & York, D. G. 2003, *Nature*, 426, 810
- Keeton, C. R. & Winn, J. N. 2003, *ApJ*, 590, 39
- Limousin, M., Richard, J., Kneib, J. ., Jullo, E., Fort, B., Soucail, G., Elíasdóttir, A., Natarajan, P., Smail, I., Ellis, R. S., Czoske, O., Hudelot, P., Bardeau, S., Ebeling, H., & Smith, G. P. 2006, *ArXiv Astrophysics e-prints*
- Macciò, A. V. & Miranda, M. 2006, *MNRAS*, 368, 599
- Mao, S. & Schneider, P. 1998, *MNRAS*, 295, 587
- Metcalf, R. B. & Zhao, H. 2002, *ApJ*, 567, L5

- Oguri, M., Inada, N., Keeton, C. R., Pindor, B., Hennawi, J. F., Gregg, M. D., Becker, R. H., Chiu, K., Zheng, W., Ichikawa, S.-I., Suto, Y., Turner, E. L., Annis, J., Bahcall, N. A., Brinkmann, J., Castander, F. J., Eisenstein, D. J., Frieman, J. A., Goto, T., Gunn, J. E., Johnston, D. E., Kent, S. M., Nichol, R. C., Richards, G. T., Rix, H.-W., Schneider, D. P., Sheldon, E. S., & Szalay, A. S. 2004, *ApJ*, 605, 78
- Raychaudhury, S., Saha, P., & Williams, L. L. R. 2003, *AJ*, 126, 29
- Ros, E., Guirado, J. C., Marcaide, J. M., Pérez-Torres, M. A., Falco, E. E., Muñoz, J. A., Alberdi, A., & Lara, L. 2000, *A&A*, 362, 845
- Saha, P. 2003, *Principles of Data Analysis* (Great Malvern, UK, Cappella Archive, 2003)
- Saha, P., Coles, J., Macciò, A. V., & Williams, L. L. R. 2006a, *ApJ*, 650, L17
- Saha, P., Read, J. I., & Williams, L. L. R. 2006b, *ApJ*, 652, L5
- Saha, P. & Williams, L. L. R. 1997, *MNRAS*, 292, 148
- . 2003, *AJ*, 125, 2769
- . 2004, *AJ*, 127, 2604
- . 2006, *ApJ*, 653, 936
- Saha, P., Williams, L. L. R., & Abdelsalam, H. M. 2001, in *ASP Conf. Ser. 237: Gravitational Lensing: Recent Progress and Future Go*, ed. T. G. Brainerd & C. S. Kochanek, 279–+
- Sharon, K., Ofek, E. O., Smith, G. P., Broadhurst, T., Maoz, D., Kochanek, C. S., Oguri, M., Suto, Y., Inada, N., & Falco, E. E. 2005, *ApJ*, 629, L73
- Trotter, C. S., Winn, J. N., & Hewitt, J. N. 2000, *ApJ*, 535, 671
- Williams, L. L. R. & Saha, P. 2004, *AJ*, 128, 2631
- Witt, H. J., Mao, S., & Keeton, C. R. 2000, *ApJ*, 544, 98
- Yoo, J., Kochanek, C. S., Falco, E. E., & McLeod, B. A. 2005, *ApJ*, 626, 51
- . 2006, *ApJ*, 642, 22
- Zekser, K. C., White, R. L., Broadhurst, T. J., Benítez, N., Ford, H. C., Illingworth, G. D., Blakeslee, J. P., Postman, M., Jee, M. J., & Coe, D. A. 2006, *ApJ*, 640, 639

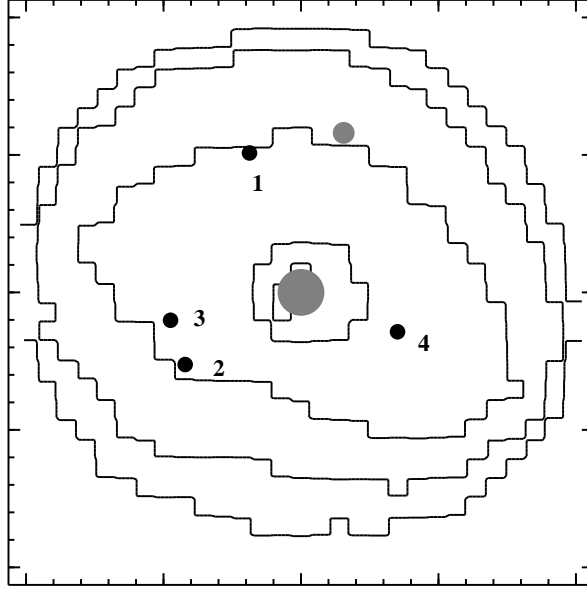


Fig. 1.— Ensemble average mass map for J0414+053. On the axes, the large ticks show 10 kpc. The mass contours are in powers of  $10^{0.4}$  (i.e., like a magnitude scale) and the third outermost contour corresponds to  $10^9 M_\odot \text{ kpc}^{-2}$ . Images are marked by small filled circles and labelled by arrival time order; 1,2,3,4 correspond to B,A1,A2,C in older papers. In fact each filled circle really corresponds to three very close image components; these are the VLBI components p,r,s shown in Fig. 2 of Trotter et al. (2000). The main lensing galaxy G and the secondary galaxy X are indicated by gray filled circles, whose radius is proportional the cube root of the flux.

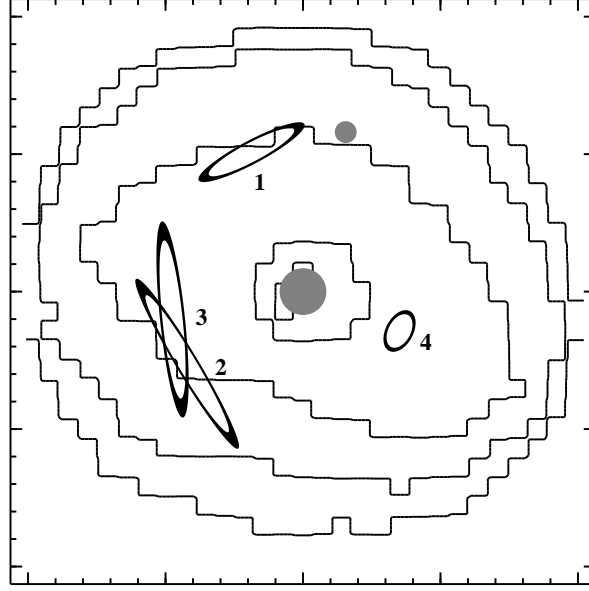


Fig. 2.— Similar to Fig. 1, but showing the inferred tensor magnifications. The ellipses indicate how a small circular source would be magnified and distorted (except that the sizes are greatly exaggerated). This figure may be compared with Fig. 3 in Trotter et al. (2000).

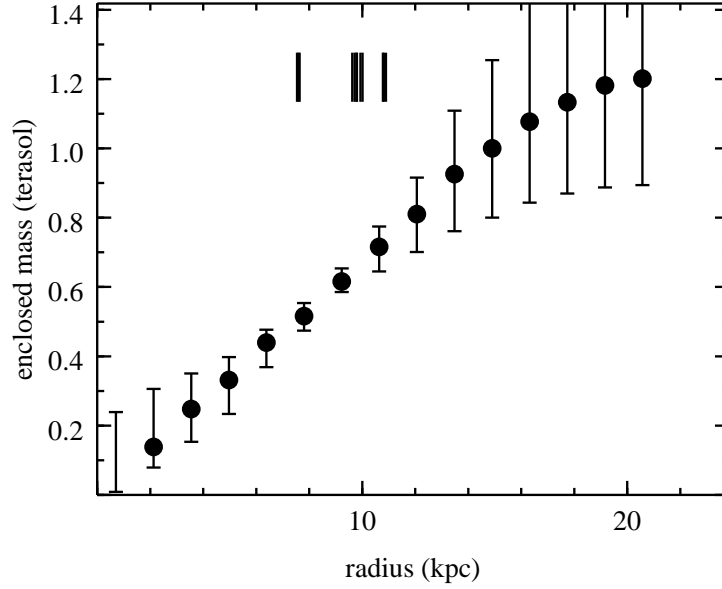


Fig. 3.— Enclosed mass of J0414+053 in  $10^{12}M_{\odot}$ . The error bars show a 90% confidence region. The barcode-like pattern indicates the image radii.



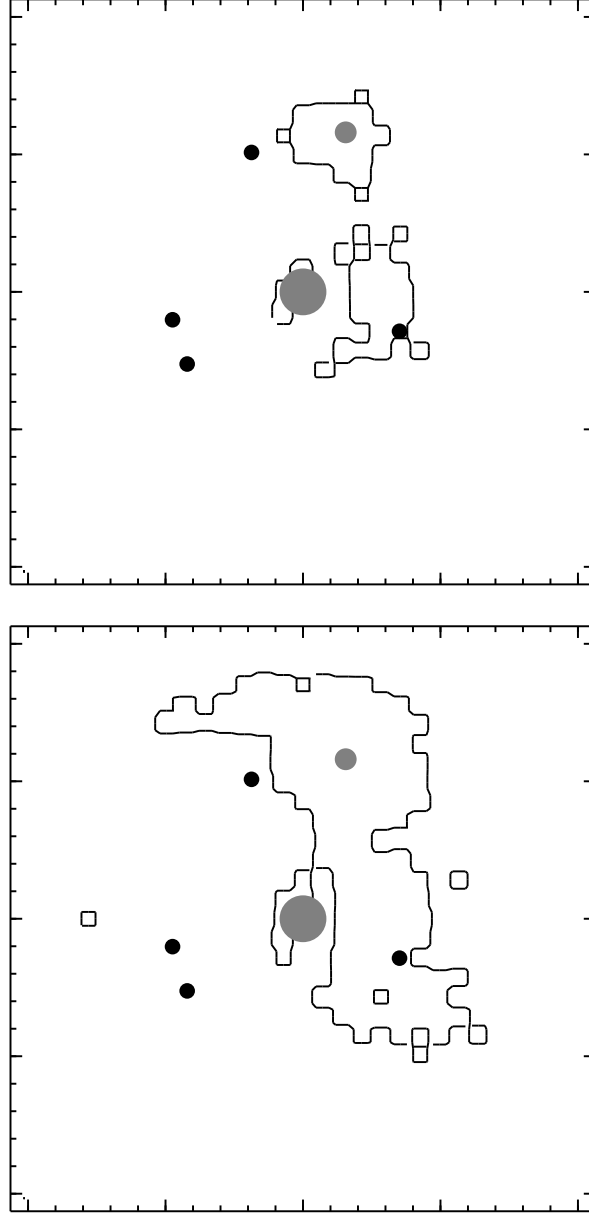


Fig. 4.— Like Fig. 1 but showing the asymmetric overdensity (see text) of J0414+053. The contours in the upper (lower) panel correspond to  $0.2$  ( $0.1$ )  $\times 10^9 M_{\odot} \text{ kpc}^{-2}$  and contain an excess mass of  $\simeq 1.7$  ( $2.5$ )  $\times 10^{11} M_{\odot}$ . The total mass (cf. Fig. 3) is  $1.2 \times 10^{12} M_{\odot}$ .

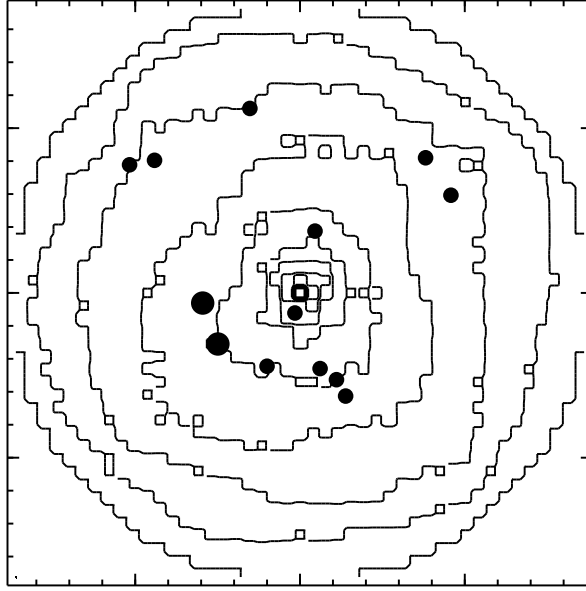


Fig. 5.— Ensemble-average mass map for J1004+411. Large ticks on the axes correspond to 100 kpc. Contour steps are  $0.5 \times 10^9 M_\odot \text{ kpc}^{-2}$ . Filled circles mark image positions. This figure is similar to the top left panel in Fig. 1 of Saha et al. (2006b), except that the short time delay (two larger circles to the SE) is constrained to be 38 days. Fig. 9 of Fohlmeister et al. (2006) also fits the time delay, but includes only one of the four multiple-image systems.

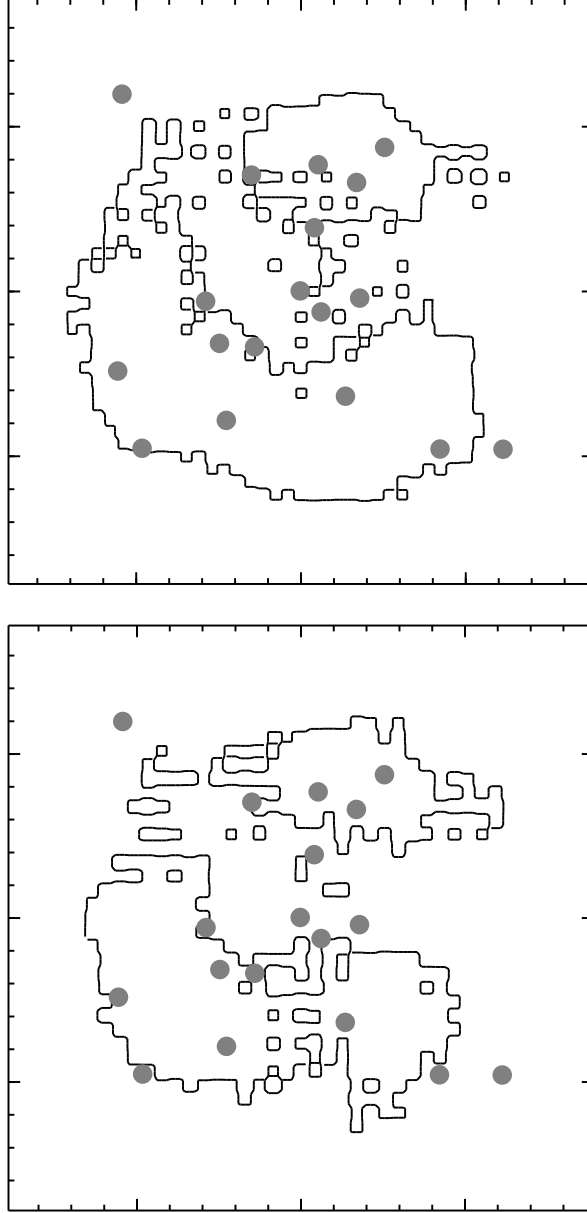


Fig. 6.— Residual mass maps of J1004+411 after subtracting off the best-fit NFW. The upper panel is derived from the model shown in Fig. 5, while the lower panel is derived from the models in Paper I. The contours show an overdensity level of  $10^8 M_\odot$  and enclose  $\simeq 7$  ( $6$ )  $\times 10^{12} M_\odot$  of excess mass in the upper (lower) panel. This substructure is  $\simeq 7\%$  ( $6\%$ ) of the total mass in the field. As in Fig. 5, large ticks on the axis show 100 kpc. Gray filled circles indicate early-type galaxies.

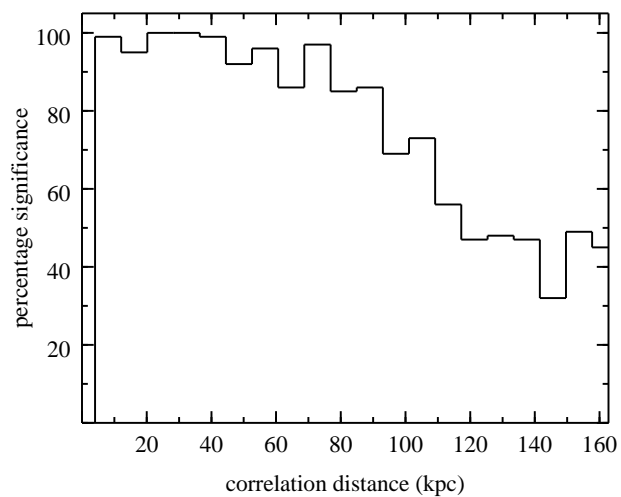


Fig. 7.— Correlation significance  $S(R)$  for galaxies against substructure in J1004+411. This refers to the models including the time delay (i.e., Fig. 5 and the upper panel of Fig. 6) but the answer for the other case is qualitatively similar.

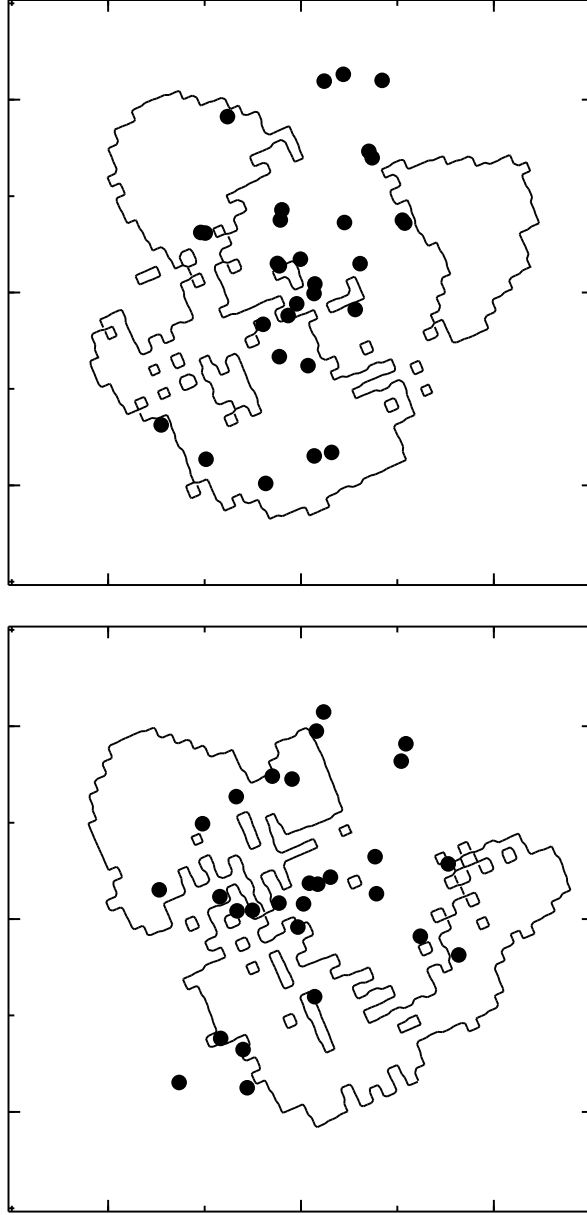


Fig. 8.— Residual mass maps of ACO 1689, using two sets of lensed images (filled circles). Large ticks on the axis show 100 kpc. In both panels, the contour denotes an overdensity level of  $2 \times 10^8 M_\odot$  and encloses  $\simeq 3 \times 10^{13} M_\odot$  of excess mass. This substructure amounts to  $\simeq 7\%$  of the total mass in the field. (This figure has the standard N-up/E-left orientation, but the mass pixel array follows the coordinate axes from Table 2 of Broadhurst et al. (2005) and these coordinate axes are discernable from the contours.)

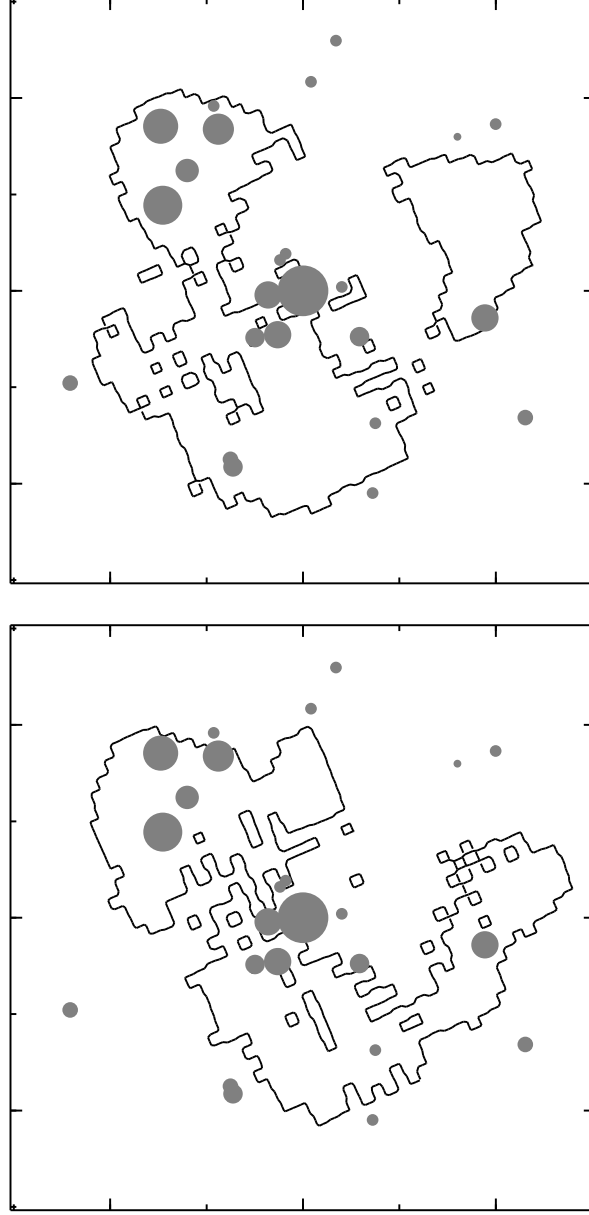


Fig. 9.— Residual map of ACO 1689 with probable cluster members shown. The contours are as in Fig. 8. Galaxies with  $B - R > 2$  are indicated by gray circles, shown with radius proportional to the cube root of the flux.

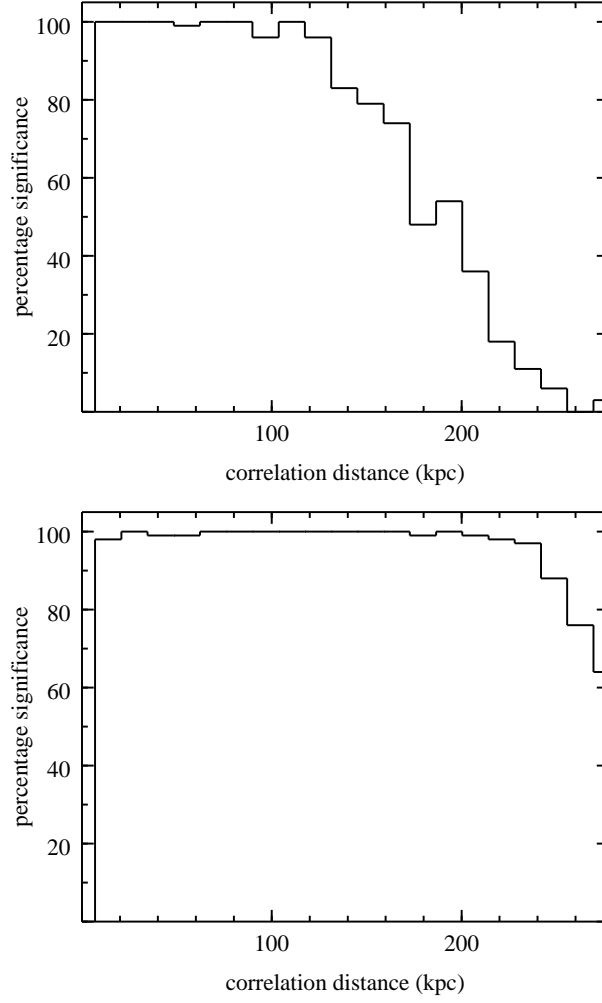


Fig. 10.— Correlation significance for flux-weighted galaxies against substructure ACO 1689. Panels correspond to panels in Fig. 9. The longer-range correlation seen in the lower panel is presumably a manifestation of the isthmus to the SW in the lower panel of Fig. 9.

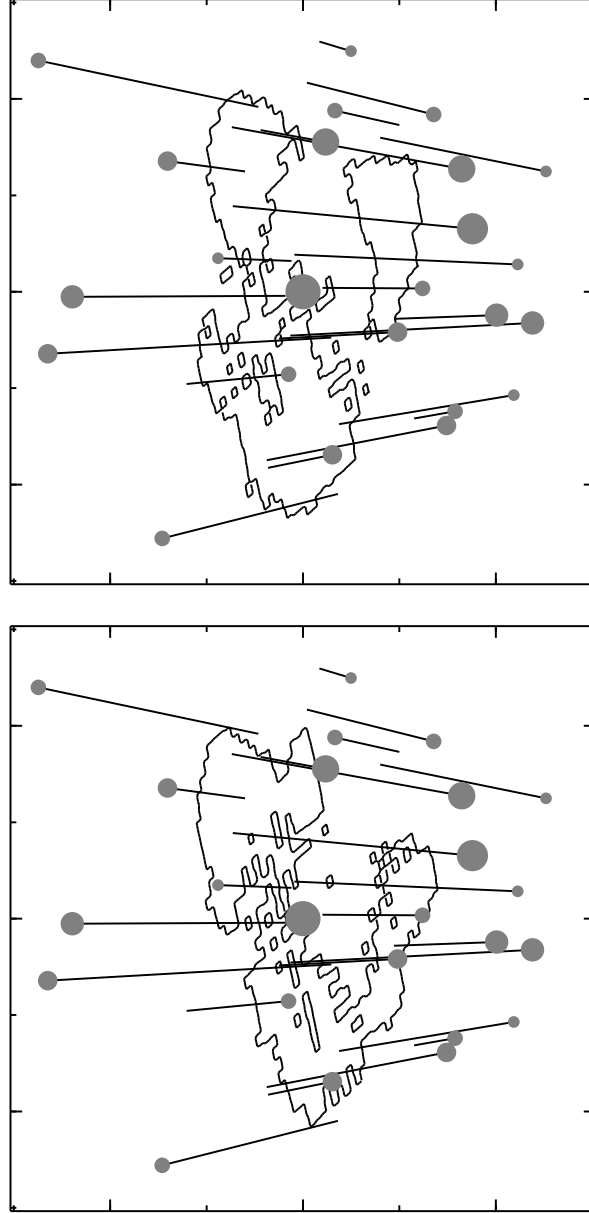


Fig. 11.— A perspective version of Fig. 9, taking the galaxy redshifts as the third coordinate. The thin lines indicate the projection of each galaxy onto the notional lens plane, which is taken to be coplanar with the brightest cluster galaxy. The range is  $\sim 500$  kpc in the spatial direction, and  $\sim 10\,000$  km/sec.



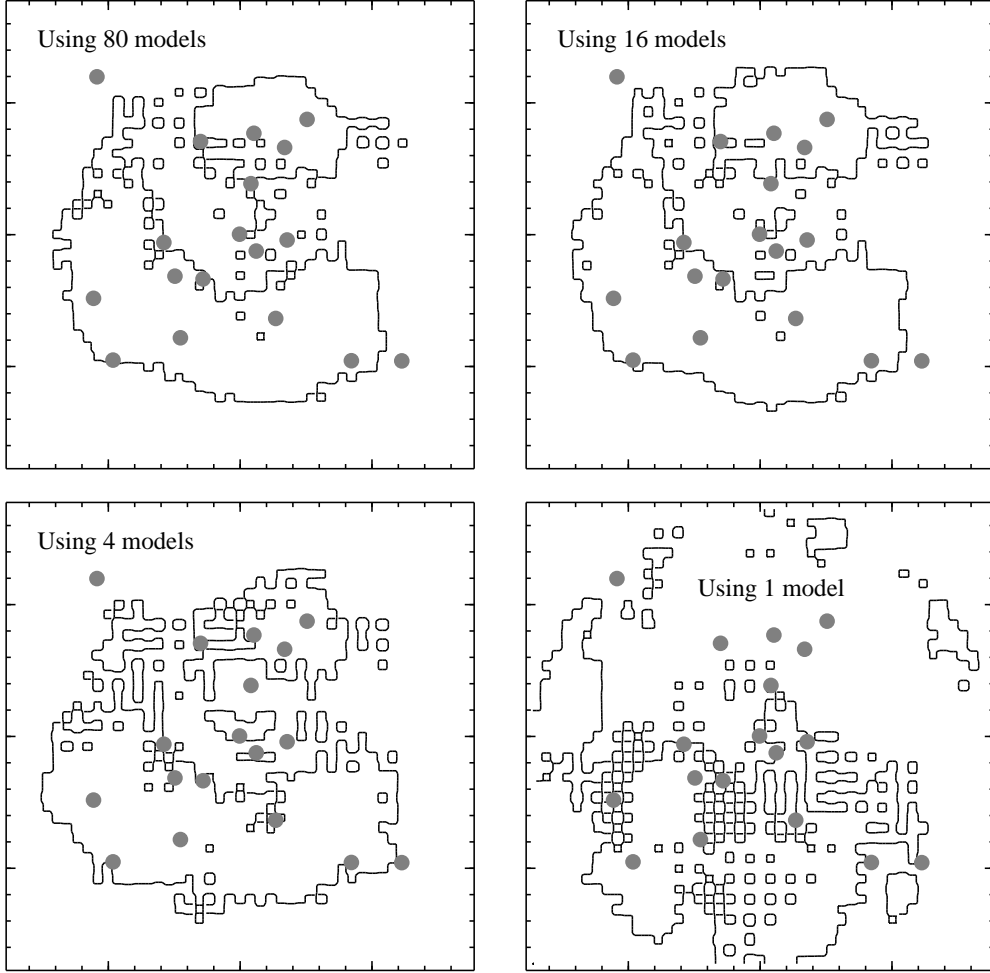


Fig. 12.— Substructure in J1004+411 derived from subsets of the model ensemble, for comparison with the full-ensemble result (i.e., using 400 models) shown in the upper panel in Fig. 6. As in the earlier figure the contours show an overdensity level of  $10^8 M_\odot$ . The excess mass enclosed within the contours is 7–8% of the total mass, the latter being consistently within a few percent of  $10^{14} M_\odot$ .